3-2-7 Remote Sensing Observations of Equatorial Plasma Bubble by HF Transequatorial Propagation

TSUGAWA Takuya, MARUYAMA Takashi, KAWAMURA Masabumi, ISHII Mamoru, and SAITO Susumu

Equatorial plasma bubbles generated in the low-latitude ionosphere after the sunset can cause scintillations and loss-of-lock of trans-ionospheric satellite signals. Continuous remote-sensing observations are effective for the nowcast and forecast of generations and propagations of plasma bubbles in the Japanese longitudinal sector. One of such remote-sensing observations is the observation of HF transequatorial propagation between Japan and Australia. This article describes the generation and propagation characteristics of plasma bubbles. The east-west asymmetry in the bottomside structures of plasma bubbles is also discussed.

1 Introduction

Röttger[1] was the first to conduct high-frequency transequatorial propagation (HF-TEP) experiments as ionospheric studies based on a direction finding technique. Kelleher and Röttger[2] compared off-great-circle HF-TEP propagations between Lindau, Germany, and Tsumeb, Namibia, with radar echoes in Nairobi, Kenya, and found a good correlation between their occurrences. Röttger[3] suggested that the large-scale structure of the equatorial ionosphere that causes off-great-circle propagation is related to the formation of equatorial spread-F (ESF) irregularities through a spatial resonance mechanism that intensifies traveling ionospheric disturbances (TID).

The onset of ESF is basically associated with plasma bubbles that are induced by Rayleigh-Taylor (R-T) instability (e.g., [4]). The nonlinear growth of R-T instability forms low-density plasma "bubbles" in the ambient high density ionospheric plasma. These bub-

bles intrude into the topside ionosphere, extending over several thousand kilometers along the magnetic field line. This phenomenon is known as "plasma bubbles". 630-nm airglow observations using an all-sky camera have identified plasma bubbles as band-like airglow depletions that extend 50 to 200 km wide in the east-west direction and more than 3,000 km long in the north-south direction (e.g., [5]). Keskinen et al.[6] demonstrated the three-dimensional structures of plasma density depletion region by a nonlinear simulation of R-T instability, thereby showing that the structures are related to the uplifts of the bottomside ionosphere along the magnetic meridian. Since the modulated isodensity surface, a bottomside structure of plasma bubbles, forms a local ionospheric tilt, it could change HF radio wave propagation paths. Thus, HF-TEP experiments could reveal local uplifts of the bottomside ionosphere associated with plasma bubbles.

One of the difficulties of transequatorial

propagation experiments is to find a suitable location pair near the conjugate points in both hemispheres. We have installed the MUSIC (multiple signal classification) directional-finder[7][8] in Oarai, Japan for our HF-TEP experiments. The MUSIC algorithm can be applied to any kind of radio wave modulation. We observe transequatorial propagation of the HF radio broadcast transmitted 24 h a day by Radio Australia from Shepparton, Australia.

This article is based in part on the study of Maruyama and Kawamura[9].

2 Experiment Setup

Broadcasting signals of Radio Australia transmitted from Shepparton (145.3° E, 36.2° S) were received at Oarai (140.6° E, 36.3° N). As shown in Fig. 1, the transmitting and receiving stations were aligned along 140–145° E longitude with the horizontal distance of ~8,000 km. The great-circle direction from Oarai to Shepparton is 175.7° clockwise from due north (4.3° eastward from due south). The HF directional-finder at Oarai consists of seven crossed-loop antennas, each being 2 m in diameter and all equally spaced along the circumference of a circle 60 m in diameter. The resolutions of elevation and

azimuth angles of direction of arrival (DOA) were 1°, and up to three different DOAs were simultaneously resolved with the time resolution of 0.5 s. HF radio broadcast are generally transmitted simultaneously with multiple frequencies, which vary depending on the local time and season as shown in Fig. 2. For this reason, the receiving frequency are scanned through all the possible frequencies (3 to 30 MHz). When the signals were detected, information about the receiving signals, such as frequency, azimuth angle, elevation angle, signal strength, is measured for 8 s. Then the next receiving frequency is scanned.

3 Results

In our HF-TEP experiment, we were most interested in the off-great-circle propagation caused by the ionospheric tilt associated with the large-scale structure of the bottomside ionosphere, and therefore analyzed temporal variations of the azimuth angle of DOAs. Figure 3 shows the DOA azimuth-time (AT) plots on April 21 to 22, 2003. The axis of abscissa is the universal time (UT) [Japan Standard Time (JST) minus 9 h], and the center of the axis corresponds to midnight in Japan. The azimuth angle measured clockwise from due north is taken on the axis of ordinates. Because multiple broadcasting stations
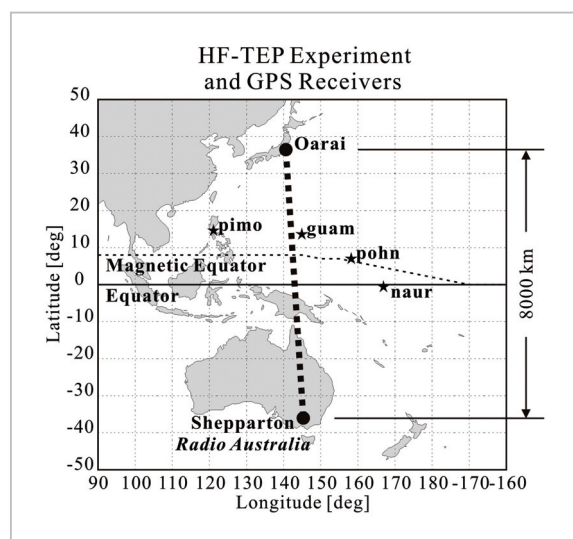

Fig.1 *Transmitting and receiving stations for the HF transequatorial propagation experiments and GPS receivers*
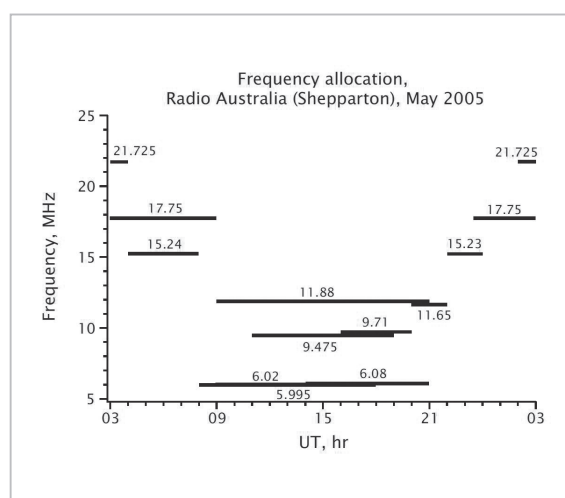

Fig.2 *Frequency allocation of Radio Australia (Shepparton) as of May 2005[9]*

generally use the same frequency to transmit HF radio broadcasts, HF signals from broadcasting stations other than Radio Australia can be noises for our experiments. However, since most of these broadcasting stations are located in the Northern Hemisphere, their radio waves can be easily distinguished in the AT plots. Data whose azimuth angle is 240° or higher (60° or higher westward from due south) in Fig. 3 and other AT plots represents interference from such other broadcasting stations.

The DOA of Radio Australia in the daytime is close to the great-circle and forms a single horizontal trace (main trace) around 176° in the AT plot. Towards sunset, the DOA of the main trace shifts somewhat westward relative to the great-circle at about 08:40 UT, returning to the normal great-circle by 09:30 UT. The trace then shifts slightly eastward and gradually reverts to the great-circle through the nighttime. Such variations in the DOA are basically repeated every day and can be understood to correspond to the ionospheric variations associated with the sunset terminator. Similarly, the DOA shifts eastward around the sunrise terminator and then gradually reverts to the great-circle. These variations are also repeated every day. A different type of trace (satellite trace) from the main trace described above appears in the AT plots for March 22 to 23, 2003 shown in Fig. 4. The satellite trace suddenly appears at 12:00 UT at azimuth angle of about 240° and then moves eastward for about 3.5 h at a constant time rate of change.

Figure 5 is the AT plots for March 24 to 25, 2004, showing the appearance of multiple satellite traces. Each of the satellite traces appearing west of the great-circle demonstrates temporal variations similar to those shown in Fig. 4. We can identify at least four traces (numbered 1 to 4) that are spaced almost evenly and shift westward with the lapse of time. Each satellite trace retains its contour for about one hour after appearing, but then gradually diffuses out of sight. The main trace is found somewhat scattered in the nighttime compared with previous two nights (Figs. 3 and 4).
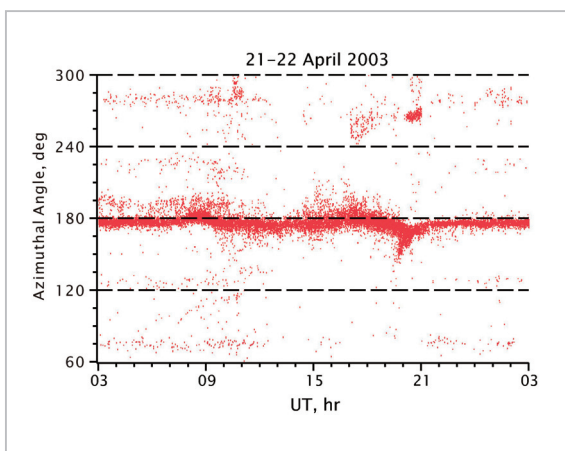

Fig.4   AT plots on March 22 to 23, 2003 (reconstructed from[9])
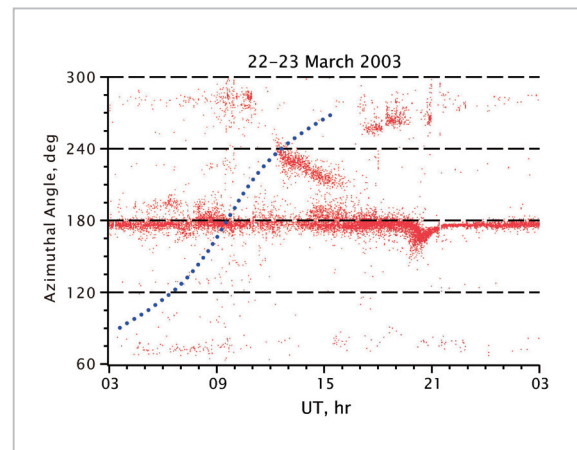

Fig.3   Azimuth-time (AT) plots on April 21 to 22, 2003 (reconstructed from[9])
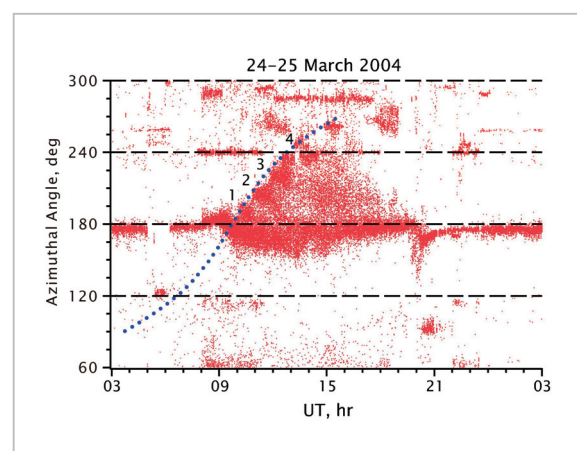

Fig.5   AT plots on March 24 to 25, 2004 (reconstructed from[9])

4 Discussions

4.1 Terminator Effect

We will first discuss the DOA deviations from the great-circle direction that appear every day in the main trace near the sunset and sunrise terminators. The ionospheric height rises rapidly at the sunset terminator under the influence of the evening enhancement or pre-reversal enhancement (PRE) of the eastward electric field in the equatorial ionosphere (e.g., [10]). Moreover, the chemical recombination of molecular ions proceeds rapidly in the bottomside ionosphere. The enhancement of the eastward electric field is known to last for about two hours neat the sunset terminator. During this period, the ionospheric height rises by 10 to 100 km or more though it largely depends on season or solar activity. Assuming that such temporal variations of ionospheric height at a given location are equivalent to the longitudinal spatial structures in the equatorial region at a given moment, the isodensity surface of the bottomside ionosphere would tilt up westward and down eastward over 3,000 km in the zonal direction. This zonal tilt causes the DOA of HF-TEP to shift westward to the great-circle. When the ionospheric layer reaches the maximum height, the DOA reverts to the great-circle direction because the isodensity surface becomes horizontal. With the subsequent lowering of ionospheric height, the isodensity surface tilts up westward and down eastward, causing the DOA to shift eastward to the great-circle direction. This westward shift following the PRE peak is smaller than the pre-peak westward shift. This could reflect the fact that the western wall of the bottomside ionospheric structure rising as a result of PRE is in the sunlit hemisphere and has a large zonal electron density gradient, on the other hand, the eastern wall has a small zonal gradient due to the recombination of molecular ions in the bottomside ionosphere on the nightside. As the height of the bottomside ionosphere reaches a state of chemical equilibrium through the nighttime, the DOA reverts

to the great-circle direction.

Near the sunrise terminator, photo-ionization due to sunshine causes a rapid increase in the electron density of the bottomside ionosphere from the eastern direction. The isodensity surface consequently tilts up westward and down eastward, resulting in the eastward shift from the great-circle direction in the DOA.

4.2 Onset Time of Satellite Trace

Assuming that satellite traces are caused by once mirror reflection of the HF-TEP on the bottomside of a plasma bubble near the equator, the local time (LT) at the reflection point can be determined from each point in the AT plot. A local uplift of the bottomside ionosphere due to a plasma bubble extends along the magnetic meridian over several thousand kilometers and has the zonal width of 50 to 200 km. The magnetic declination angle is close to 0° in the equatorial region in Southeast Asia. Thus, we consider a north-south aligned linear structure model as indi-
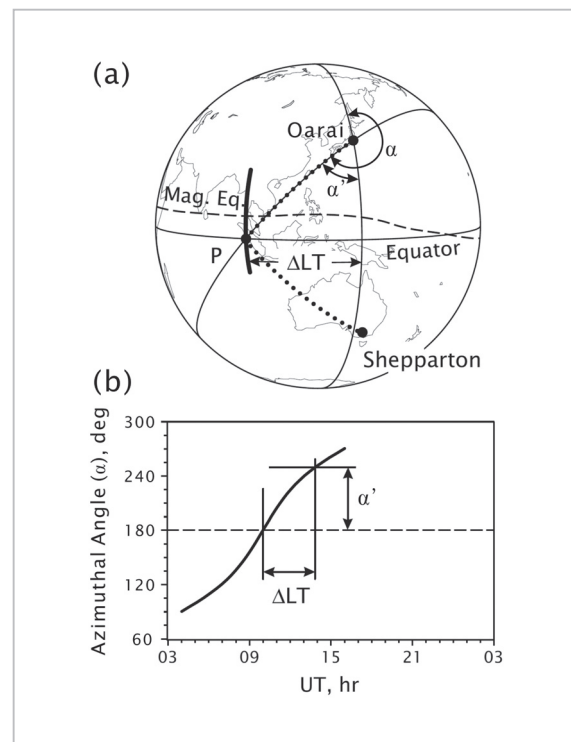

Fig.6 *Relationship between the azimuth direction of arrival of HF-TEP and reflection point P (reconstructed from [9])*

cated by a bold line in Fig. 6a. Because Shepparton and Oarai are almost conjugate points in a system of geographic coordinates, reflection point P of the HF-TEP is assumed to lie on the geographic equator. The longitude of point P can be determined from azimuth angle a at Oarai. The LT at the reflection point or the location of the plasma bubble can then be determined from the longitudinal width between Oarai and point P, together with the UT when a signal is received. In the AT plot, reflection point P fixed at the LT follows an S-shaped track (S-curve) as shown in Fig. 6b. The UT when the S-curve passes azimuth angle $\alpha=180°$ is the LT at Oarai's meridian.

In Figs. 4 and 5, the S-curve tangent to the satellite trace passes $\alpha=180°$ at 09:45 UT (19:05 LT). Figure 7 shows a superimposition of all the AT plots in which a satellite trace appears during March 2003. In the west of the main trace close to the great-circle direction, the upper-left boundary of the satellite traces is well aligned with the S-curve, indicating that the onset of individual satellite traces is at the same LT. This corresponds to that plasma bubbles are mainly generated around sunset[11]. The white dotted line in Fig. 7 represents an average main trace. The S-curve intersects the main trace when it reverts to the great-circle direction after the westward shift associated with the uplift of the ionospheric height around the sunset terminator. In other words,

the satellite trace starts when the ionospheric height reaches the maximum. This is consistent with the plasma bubbles observed by radar backscatter echoes that often start when the ionospheric layer is at its peak height or the layer is descending[12]. From another viewpoint, the agreement of the beginning of a satellite trace with the S-curve may well attest to the validity of the assumption that the reflection point of HF-TEP is located on the geographical equator. If the reflection point is located north (or south) of the equator, azimuth angle a in relation to the same plasma bubble should increase (or decrease).

4.3 Drift Velocity and Spatial Structure

In the AT plots, the satellite trace is moving eastward. The east-west drift velocity of the event observed on March 22 to 23, 2003, is estimated using the method illustrated in Fig. 8. First, two reference points are put on a satellite trace (slanted bold line) to designate the beginning of the satellite trace and its status 60 minutes later. Two S-curves are then drawn to pass these two reference points. Compared with the actual time difference of 60 minutes observed at Oarai, there is an LT difference of 92 minutes between the two S-curves at the reflection point. The 32-minute difference attributes to the eastward drift of the reflection point, which corresponds to 8° longitude or a zonal distance of 890 km.
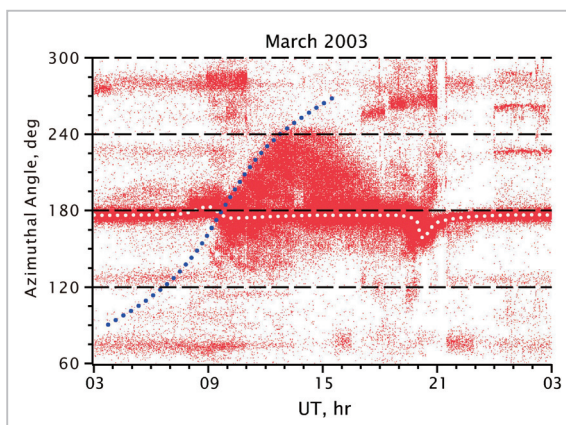
Fig.7 Superimposition of all the AT plots in which a satellite trace appears during March 2003 (reconstructed from[9])
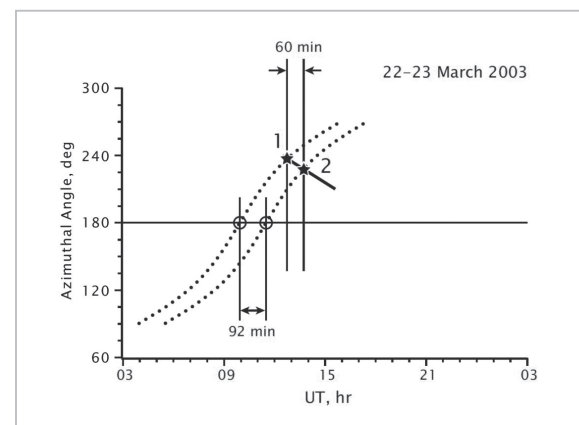
Fig.8 Method of estimating the east-west drift velocity of a plasma bubble that forms a satellite trace (reconstructed from[9])
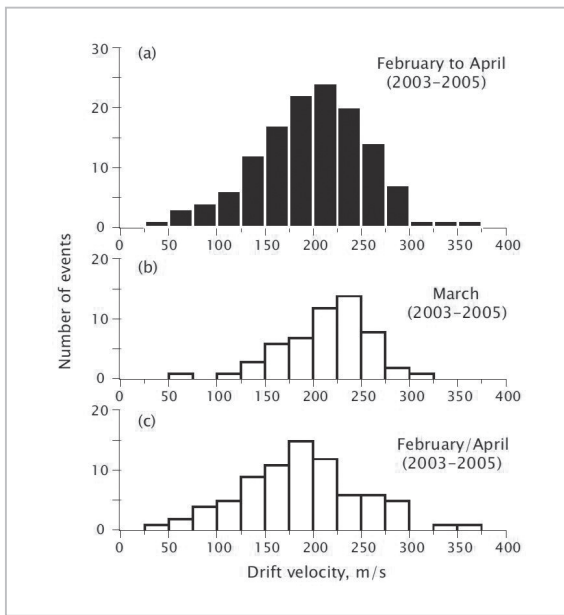
Fig.9 *Drift Velocity and Spatial Structure*[9]

Hence, the plasma bubble represented by this satellite trace has been estimated to have the eastward drift velocity of 247 m s^{-1}, though the velocity may include errors of 7–8 m s^{-1} even in the case of the clear trace[13].

Using this method, the east-west drift velocity of plasma bubbles was calculated during the seasons around March in which satellite traces are frequently observed. Figures 9a-c show the east-west drift velocities (positive eastward) during February to April in 2003 to 2005, during March when satellite traces frequently occur, and during February and April, respectively. The drift velocity varies from month to month. The median value in the high occurrence month reaches as high as 220 m s^{-1} and that in the other months is 190 m s^{-1}. The median value in the entire months is 200 m s^{-1} (Fig. 9a). The east-west drift velocity of a plasma bubble is considered to be essentially determined by that of the background ionospheric plasma or neutral wind velocity. The east-west drift velocity estimated using this method with HF-TEP experiments is comparable with that of plasma bubbles observed in the Indian longitudinal sector by the FUV imager onboard the IMAGE satellite[14]. In addition, Saito et al.[13] have also revealed good agreement between the drift velocity of plasma bubbles estimated by this method and the drift velocity of ionospheric irregularities within the plasma bubbles estimated by GPS scintillation observations. On the other hand, the east-west drift velocity of plasma bubbles observed by the ROCSAT-1 satellite[15], the average ionospheric plasma drift velocity observed by the Jicamarca radar in Peru, and the neutral wind velocity observed by the DE-2 satellite[16] show lower values than the drift velocities estimated by this method based on the HF-TEP observations. To discuss the quantitative differences in more detail, it is needed to consider that the longitude dependence of the drift velocity of plasma bubbles[14], the possibility that the reflection point of HF-TEP deviates from the geographical equator latitude (e.g., the geomagnetic equator), or the possibility of multiple reflection points. Moreover, since the plasma drift velocity varies at different ionospheric heights, the sensible height may differ depending on the methods of observation, which may result in the different drift velocities. A more quantitative discussion of plasma drift velocities could be possible by HF-TEP experiments between two geomagnetic conjugate points and ground-based observations near the reflection point simultaneously.

As for the multiple event on March 24 to 25, 2004 (as shown in Fig. 5), the drift velocity of plasma bubbles was estimated at 232 m s^{-1}. Using this velocity, the wavelength of the periodic satellite traces can be estimated. The individual satellite traces start at the same LT, with a interval of 50 minutes in their start time (UT). During this 50-minute period, the location where the next plasma bubbles starts is shifted 1,390 km westward, with the first plasma bubble drifting 700 km eastward. Hence, the two plasma bubbles are estimated to be 2,090 km apart in the east-west direction. This wavelength is comparable with large-scale TIDs observed at mid-latitudes during magnetic disturbances. Plasma bubbles identified by HF-TEP observations conducted by Röttger[1] and by FUV imaging observations by the IMAGE satellite have wavelengths

comparable with medium-scale TIDs (several hundreds to 1,000 km). In our HF-TEP experiments, as shown in the AT plots of Fig. 5, the satellite traces are often obscure at a later LT. This may be attributable to the existence of narrow-spaced multiple plasma bubbles and/or the bifurcation of a single large-structured plasma bubble[17]. Because our HF-TEP experiments assume mirror reflection on the bottomside ionosphere, if the bottomside ionosphere contains smaller-scale structures, their scattering effect would not be removable. Since the equatorial ionospheric structure is considered to involve various spatial scales, different observation methods are likely to be sensitive to different wavelengths.

4.4 Seasonal Variation

Figure 10 shows the monthly occurrence of satellite trace and the monthly averages of the solar flux index (F10.7). The monthly occurrence is defined as the number of days on which one or more satellite traces were observed in each month. The occurrence of satellite traces is essentially limited to February through April and the seasons around October. Seasonal variations in the occurrence of plasma bubbles are known to depend on longitude. In regions with a low magnetic declination, such as Southeast Asia and India, the occurrence of ESF or plasma bubbles is large around the equinoctial seasons[18]. Similar seasonal variations can also be noted in the number of occurrences of GHz-band scintillations in the equatorial region[19]-[21].

In addition to the general equinoctial maxima, Fig. 10 also shows a spring/autumn asymmetry of the number of plasma bubble occurrences, that is larger in spring (February to April) than in autumn (around October). This seasonal asymmetry of plasma bubbles is not clearly seen in the seasonal longitudinal variation diagram of plasma bubble occurrence frequency based on the DMSP satellite observations from 1989 to 2002[22]. The magnitude of the spring/autumn symmetry varies from year to year and, for example, was outstanding in 2003 but less evident in 2004. A
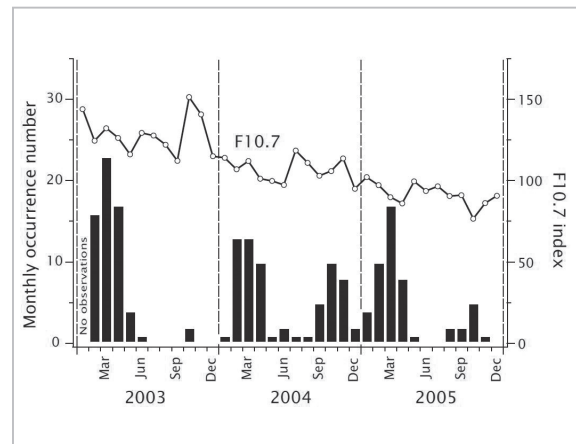
Fig.10 Monthly occurrence of satellite trace and the solar flux index (F10.7)[9]

transequatorial propagation experiment in the VHF band between Yamagawa, Japan, and Darwin, Australia, has also revealed similar seasonal variations and spring/autumn asymmetry observed in the signal reception rate[23]. This VHF-TEP experiment also revealed strong spring/autumn asymmetry in some years but rarely in others. The VHF-TEP is associated with forward scattering caused by ionospheric irregularity or duct propagation in the plasma bubbles[24]. Figure 10 shows the F10.7 index changes from 130 to 80 over the three-year period from 2003 to 2005, suggesting gradually declining solar activity. Except for the seasons around the autumn of 2003, the occurrence number of satellite trace has been gradually declining from year to year similar to the solar activities. This trend is consistent with the trend of the occurrences of sharp electron density depletions at a height of 800 km observed by the DMSP satellite[25].

4.5 Bottomside Structure of Plasma Bubble

As shown in Fig. 7, satellite traces often appear to the west of the main trace (upper side of AT plot) but seldom to the east. This could attribute to the absence of plasma bubbles to the east of the great-circle direction, that is the east-west asymmetry of plasma bubble occurrences, or the existence of the east-west asymmetry of the bottomside struc-
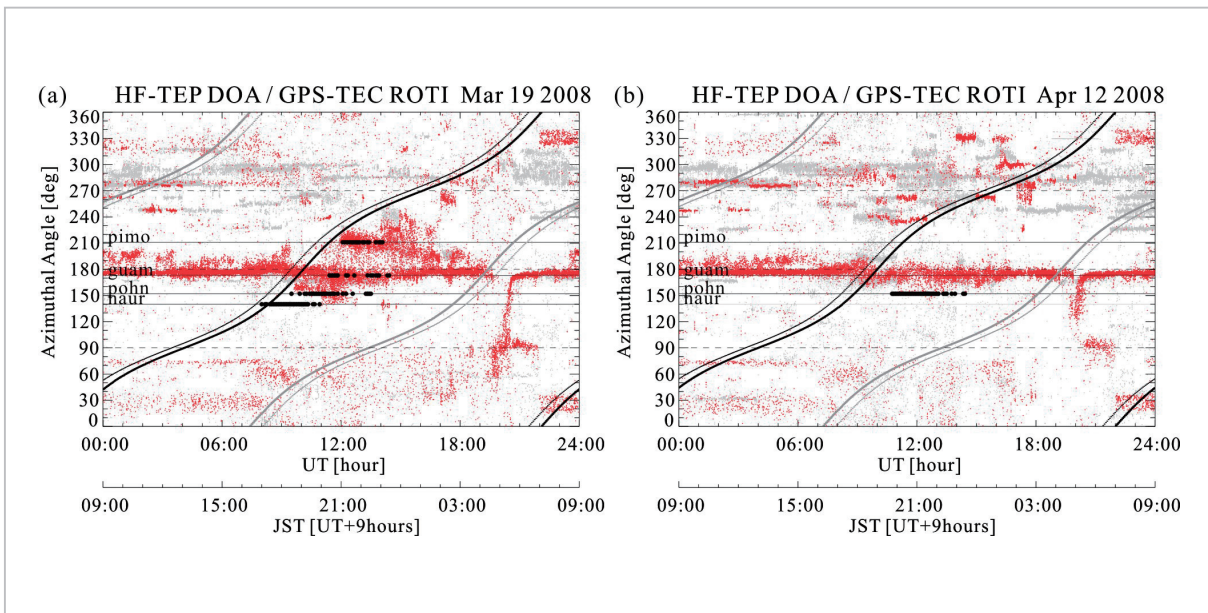
tures of plasma bubbles. The former east-west asymmetry is not likely to attribute to that of satellite-trace appearances because the Oarai-Shepparton great-circle path has been established just for the sake of circumstances of our HF-TEP observations. We should, however, verify this possibility by using a method other than HF-TEP to eliminate it completely.

The total electron content (TEC) was derived from the four GPS receivers (pimo, guam, pohn and naur as shown by stars in Fig. 1) located in the Western Pacific equatorial region to investigate the east-west asymmetry of plasma bubble occurrences on both sides of the Oarai-Shepparton great-circle path. Standard deviations of rate of TEC change per minute (dTEC/min) with 5-minute window were then calculated from the 30-second TEC data derived from each GPS receiver-satellite pair[26]. This value is called ROTI (rate of TEC change index) and is often used as an index for the ionospheric disturbances with a spatial scale of ~20 km. In the equatorial region, the ROTI enhancement is considered to be associated with small-scale ionospheric irregularity in a plasma bubble. Thus, the ROTI index is also used as an indicator of plasma bubble occurrence (e.g., [26]). In the AT plot for March 19, 2008 shown in Fig. 11a,

black dots represent the periods during which the median value of ROTI is 1 TECU/min (1 TECU=10^{16} m^{-2}) or more at each receiver location. The azimuth angle of each GPS receiver in the AT plot is defined as that of the geographic equator at the same longitude as the receiver. The black (gray) fine and bold S-curves in Fig. 11a designate the azimuth angles at sunset (sunrise) at geographic equator at the ionospheric heights of 100 km and 400 km, respectively. In the AT plot in Fig. 11a, satellite traces start around 160° at 09:30 UT and around 220° at 12:00 UT, and then shift eastward with the lapse of time. Increases in ROTI are observed at pimo, guam, and pohn GPS receivers while the satellite traces appear. At naur, however, the enhancement in ROTI was observed after sunset but no associated satellite trace is identified. Figure 11b shows the AT plot for April 12, 2008. No remarkable satellite trace was observed in this AT plot, but enhancements in ROTI at pohn were observed from 10:00 UT after sunset. Unfortunately, there is no observation data at naur for this day. The two events in Fig. 11 indicate that the enhancements in ROTI in the west of the great-circle path accompany with satellite trace occurrences, on the other hand, satellite traces do not always appear in the east of the great-circle path even
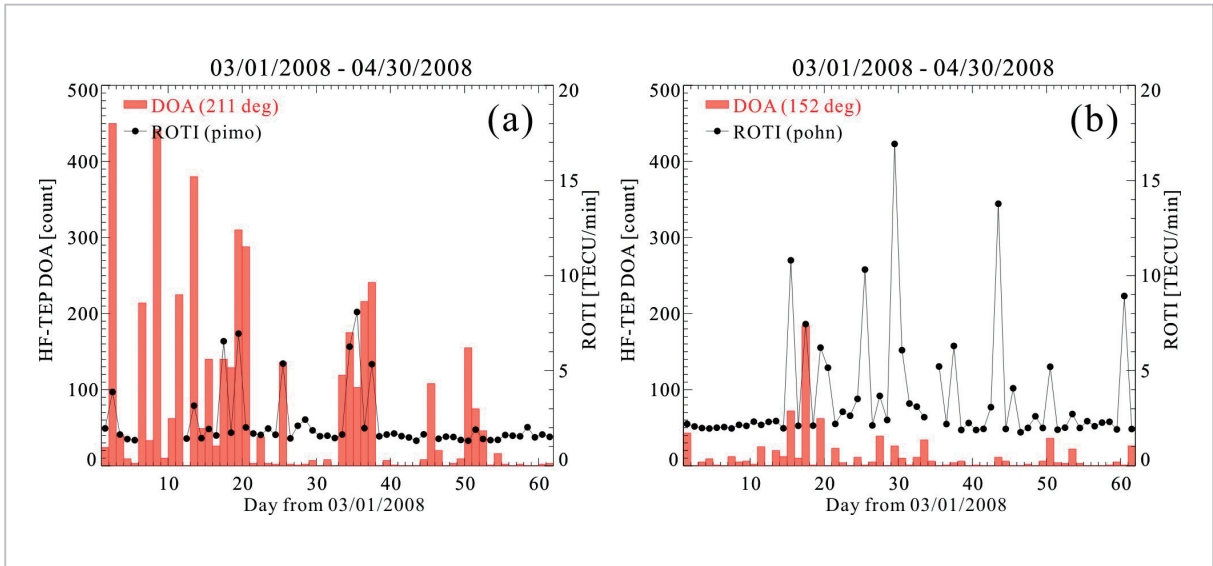
Fig.12 Day-to-day variations in HF-TEP direction of arrival count and enhancements in ROTI at azimuth angles of 211° (pimo) and 157° (pohn)

if the enhancements in ROTI are observed.

Figure 12 shows the day-to-day variations in the sum of the HF-TEP direction of arrival (DOA) count and ROTI at azimuth angles of (a) 221° (pimo) and (b) 157° (pohn) from the sunset to the midnight. Although both HF-TEP and ROTI have large day-to-day variations, satellite traces are observed in all eight events in which enhancements in ROTI are observed at the azimuth angle of 211° (pimo) to the west of the great-circle path. On the other hand, satellite traces appear in only five out of the 13 events in which enhancements in ROTI are observed at the azimuth angle of 157° (pohn) to the east of the great-circle path. These observational results indicate that few appearances of satellite traces in the east of the great-circle path would result from the east-west asymmetry of the bottomside structures of plasma bubbles rather than that of plasma bubble occurrences.

Before the discussions of why satellite traces are likely to appear in plasma bubbles west of the great-circle path, we should review the physical mechanisms of off-great-circle propagation of HF-TEP. The candidates for the possible mechanism are the following three physical mechanisms:
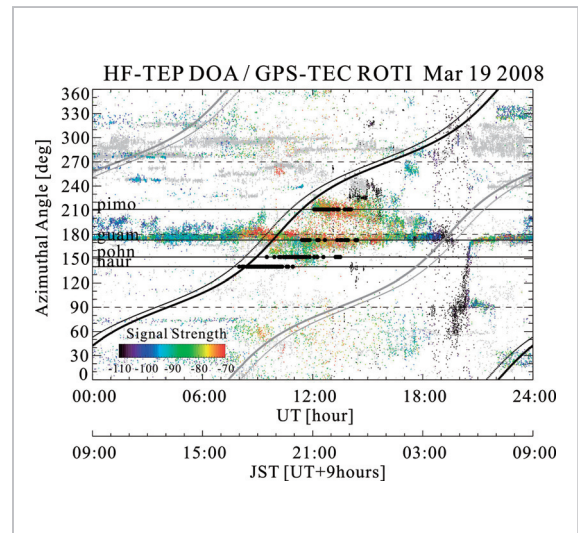
1. Mirror-reflection on the isodensity surface

Fig.13 Azimuth-time-signal strength plot for March 19, 2008

of the bottomside ionospheric F-region[1]
2. Forward scattering caused by ionospheric irregularity[23]
3. Duct propagation in plasma bubbles[24]

Figure 13 shows the same AT plot for March 19, 2008 given in Fig. 11a except that the data are plotted in different colors according to received signal strength. The satellite trace starting at 12:00 UT around 220° west of the great-circle has the comparable signal strengths with the main trace. Hence, it would
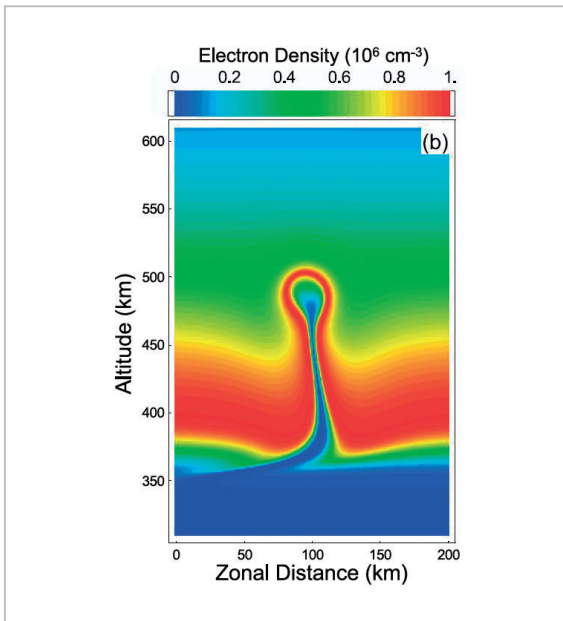
Electron Density (10⁶ cm⁻³)

Fig.14 *Simulated east-west asymmetry of the bottomside structure of a plasma bubble*[27]

be difficult to consider the satellite trace is caused by the scattering due to the ionospheric irregularity. Duct propagation in plasma bubbles is also unlikely to cause the satellite traces because the DOA of the off-great-circle propagations (west of the great-circle) is not aligned along the geomagnetic field line. Thus, the satellite trace is considered attributable to mirror reflection on the bottomside ionosphere in the same way as the main trace.

Bernhardt[27] demonstrates the east-west asymmetry on the bottomside of plasma bubbles by a computer simulation as shown in Fig. 14. This east-west asymmetry is produced by the height variations of the ion drift velocity in the east-west direction, which is basically due to those of the east-west velocity of the background neutral wind. The east-west asymmetry of the appearances of off-great-circle HF-TEP would be caused by the mirror reflection at such bottomside structures of a plasma bubble.

5 Conclusions

We have conducted the HF transequatorial propagation (HF-TEP) experiments using the HF radio broadcast of Radio Australia from Shepparton and the HF directional-finder at Oarai. Off-great-circle HF-TEP (satellite trace) often observed at nighttime reflects the uplift of the bottomside ionosphere associated with plasma bubbles. The characteristics of plasma bubbles revealed by this study, such as the time of satellite trace occurrence, zonal drift velocities, seasonal variations and east-west asymmetry of the bottomside structure, are consistent with the results of previous studies. However, some characteristics are still not quantitatively clarified, such as the eastward drift velocities of equatorial ionospheric disturbances and the spatial interval between two or more plasma bubbles. This experiment is able to observe satellite traces up to 60° west of the great-circle direction. Because plasma bubbles and associated ionospheric disturbances (such as ionospheric scintillation) generally travel eastward, this experiment makes it possible to observe a wide range of ionospheric disturbance phenomena occurring upstream. This feature made the experiment a very useful tool for monitoring and forecasting space weather phenomena that can cause radio communication failures and degrade GNSS positioning/navigation accuracy. Assuming the geographical equator to be a reflection point of the HF-TEP as used in this experiment can cause significant error in the accuracy of the zonal drift velocity of plasma bubbles. To resolve this problem, it would be necessary to conduct an HF-TEP experiment with a fixed frequency using dedicated transmitters installed at the geomagnetic conjugate point. HF-TEP ray-tracing calculations using a high-precision ionospheric model would also be useful.

Acknowledgements

References

1 Röttger, J., "Wave-like structures of large-scale equatorial spread-F irregularities," J. Atmos. Terr. Phys., Vol. 35, pp. 1195–1206, 1973.

2 Kelleher, R. F. and Röttger, J., "Equatorial spread-F irregularities observed at Nairobi and on the transequatorial path Lindau-Tsumeb," J. Atmos. Terr. Phys., Vol. 35, pp. 1207–1211, 1973.

3 Röttger, J., "The macro-scale structure of equatorial spread-F irregularities," J. Atmos. Terr. Phys., Vol. 38, pp. 97–101, 1976.

4 Fejer, B. G. and Kelley, M. C., "Ionospheric irregularities," Rev. Geophys. Space Phys., Vol. 18, pp. 401–454, 1980.

5 Weber, E. J., Buchau, J., and Moore, J. G., "Airborne studies of equatorial F layer ionospheric irregularities," J. Geophys. Res., Vol. 85, pp. 4631–4641, 1980.

6 Keskinen, M. J., Ossakow, S. L., and Fejer, B. G., "Threedimensional nonlinear evolution of equatorial ionospheric spread-F bubbles," Geophys. Res. Lett., Vol. 30, No. 16, 1855, doi: 10.1029/2003 GL017418, 2003.

7 Shumidt, R. O., "Multiple emitter location and signal parameter estimation," IEEE Trans. Antennas Propagat., Vol. AP-34, pp. 276–280, 1986.

8 Hawlitschka, S., "Travelling ionospheric disturbances (TIDs) and tides observed by a super-resolution HF direction finding system," J. Atmos. Solar-Terr. Phys., Vol. 68, pp. 568–577, 2006.

9 Maruyama, T. and M. Kawamura, "Equatorial ionospheric disturbance observed through a transequatorial HF propagation experiment," Ann. Geophys., Vol. 24, pp. 1401–1409, 2006.

10 Fejer, B. G., de Paula, E. R., Batista, I. S., Bonelli, E., and Woodman, R. F., "Equatorial F region vertical plasma drifts during solar maxima," J. Geophys. Res., Vol. 94, pp. 12049–12054, 1989.

11 Yokoyama, T., Fukao, S., and Yamamoto, M., "Relationship of the onset of equatorial F region irregularities with the sunset terminator observed with the Equatorial Atmosphere Radar," Geophys. Res. Let., Vol. 31, L24804, doi: 10.1029/2004GL021529, 2004.

12 Argo, P. E. and Kelley, M. C., "Digital ionosonde observations during equatorial spread F," J. Geophys. Res., Vol. 91, pp. 5539–5555, 1986.

13 Saito, S., T. Maruyama, M. Ishii, M. Kubota, G. Ma, Y. Chen, J. Li, C. Ha Duyen, and T. Le Thurong, "Observations of small- to large-scale ionospheric irregularities associated with plasma bubbles with a transequatorial HF propagation experiment and spaced GPS receivers," J. Geophys. Res., Vol. 113, A12313, doi: 10.1029/2008JA013149, 2008.

14 Immel, T. J., Frey, H. U., Mende, S. B., and Sagawa, E., "Global observations of the zonal drift speed of equatorial ionospheric plasma bubbles," Ann. Geophys., Vol. 22, pp. 3099–3107, 2004.

15 Lin, C. S., Immel, T. J., Yeh, H.-C., Mende, S. B., and Burch, J. L., "Simultaneous observations of equatorial plasma depletion by IMAGE and ROCSAT-1 satellites," J. Geophys. Res., Vol. 110, A06304, doi: 10.1029/2004JA010774, 2005.

16 Fejer, B. G., Kudeki, E., and Farley, D. T., "Equatorial F region zonal plasma drifts," J. Geophys. Res., Vol. 90, pp. 12249–12255, 1985.

17 Mendillo, M. and Baumgardner, J., "Airglow characteristics of equatorial plasma depletions," J. Geophys. Res., Vol. 87, pp. 7641–7652, 1982.

18 Maruyama, T. and Matuura, N., "Longitudinal variability of annual changes in activity of equatorial spread F and plasma bubbles," J. Geophys. Res., Vol. 89, pp. 10903–10912, 1984.

19 Paulson, M. R., "Scintillation of VHF/UHF and L band satellite signals at Guam," Radio Sci., Vol. 16, pp. 877–884, 1981.

20 Fang, D. J. and Liu, C. H., "A morphological study of gigahertz equatorial scintillations in the Asian region," Radio Sci., Vol. 18, pp. 241–252, 1983.

21 Otsuka, Y., K. Shiokawa, and T. Ogawa, "Equatorial ionospheric scintillations and zonal irregularity drifts observed with closely-spaced GPS receivers in Indonesia," J. Meteor. Soc. Japan, Vol. 84A, pp. 343–351, 2006.

22 Burke, W. J., L. C. Gentile, C. Y. Huang, C. E. Valladares, and S. Y. Su, "Longitudinal variability of equatorial plasma bubbles observed by DMSP and ROCSAT-1," J. Geophys. Res., Vol. 109, doi: 10.1029/2004JA010583, 2004.

23 Tanohata, K., Kuriki, I., Iguchi, M., Yamashita, K., and Sakamoto, T., "The results of long-term experiment of trans-equatorial VHF wave propagation," Rev. Radio Res. Lab., Vol. 26, pp. 885–897, 1980. (in Japanese)

24 Heron, M. L., "Recent progress in transequatorial propagation – review," J. Atmos. Terr. Phys., Vol. 43, pp. 597–606, 1981.

25 Huang, C. Y., Burke, W. J., Machuzak, J. S., Gentile, L. C., and Sultan, P. J., "Equatorial plasma bubbles observed by DMSP satellites during a full solar cycle: Toward a global climatology," J. Geophys. Res., Vol. 107, No. A12, 1434, doi: 10.1029/2002JA009452, 2002.

26 Nishioka, M., A. Saito, and T. Tsugawa, "Occurrence characteristics of plasma bubble derived from global ground-based GPS receiver networks," J. Geophys. Res., Vol. 113, A05301, doi: 10.1029/2007 JA012605, 2008.

27 Bernhardt, P. A., "Quasi-analytic models for density bubbles and plasma clouds in the equatorial ionosphere: 2. A simple Lagrangian transport model," J. Geophys. Res., Vol. 112, A11310, doi: 10.1029/2007 JA012287, 2007.

TSUGAWA Takuya, *Ph.D.*

Expert Researcher, Space Environment Group, Applied Electromagnetic Research Center

Upper Atmosphere Physics

MARUYAMA Takashi, *Ph.D. (Eng.)*

Executive Researcher

Upper Atmospheric Physics

KAWAMURA Masabumi

Former : Technical Expert, Space Environment Group, Applied Electromagnetic Research Center

Computer Network

ISHII Mamoru, *Dr. Sci.*

Director, Project Promotion Office, Applied Electromagnetic Research Center

Upper Atmospheric Physics

SAITO Susumu, *Ph.D.*

Senior Researcher, Communication, Navigation, and Surveillance Department, Electronic Navigation Research Institute

Aeronomy, Satellite Navigation